Available online at www.sciencedirect.com
SCIENCE DIRECT®
Journal of the European Ceramic Society 25 (2005) 1431–1439
www.elsevier.com/locate/jeurceramsoc

Molecular dynamics simulations of basal and pyramidal system edge dislocations in sapphire

C.T. Bodur [1], J. Chang, A.S. Argon *

Department of Mechanical Engineering, Massachusetts Institute of Technology, Room 1-306, 77 Massachusetts Avenue, Cambridge, MA 02139-4307, USA

Available online 19 February 2005

Abstract

Directionally solidified ceramic eutectics containing alumina as a topologically continuous majority component with, e.g., yttria-stabilized cubic-zirconia or with YAG as minority components have become of considerable interest as members of a new family of potential high temperature structural materials. The attractive creep resistance of such eutectics in fiber-form is based on their remarkably tight [0 0 0 1] texture of the alumina component in which neither the basal plane nor the prism plane can be activated to result in glide that can extend the eutectic by creep in tension. Under such conditions creep in such eutectics must be governed by climb of the $(1/3)\langle\bar{1}101\rangle$ edge dislocations out of either the $(11\bar{2}0)$ prism plane or the $(1\bar{1}02)$ pyramidal plane.

To develop better understanding of the core structure of these dislocations and their potential role in the creep resistance of the alumina component in eutectics with tight [0 0 0 1] textures, a molecular dynamics (MD) simulation was carried out of the comparative core structures of both the $(1/3)\langle 2\bar{1}\bar{1}0\rangle$ basal edge dislocations and the $(1/3)\langle\bar{1}101\rangle$ pyramidal edge dislocations on the $(1\bar{1}02)$ plane in sapphire. The MD simulation revealed that the equilibrium structure of the core of the pyramidal edge dislocations undergo a dissociation into two half strength partial edge dislocations displaced vertically out of the best glide plane of cation holes with weak covalent bonding and possible fair glide resistance into two adjacent pyramidal planes of very strong covalent bonding, and consequent, very high glide resistance. While this explains the immobility in glide of such dislocations on the pyramidal system, no important structural impediment was found for their climb motion out of the pyramidal planes.

Keyword: Dislocations, sapphire

1. Introduction

In the quest for materials development for more efficient power systems capable of operating at higher temperatures, it becomes necessary to go beyond the present superalloys and intermetallic compounds, which "plateau-out" at around 1000 °C, to consider oxides, nitrides, carbides and the like.[1] These, however, are all intrinsically brittle,[2] have low fracture toughness in monolithic form,[3] and at least in polycrystalline form usually suffer from excessive diffusional creep due to grain boundary diffusion and sliding.[4] In comparison, single crystal sapphire fibers of *c*-axis orientation which keep the principal basal and prismatic slip and twinning systems unstressed exhibit excellent creep resistance up to 1600 °C,[5] but still suffer from inadequate fracture toughness.[6] While use of such fibers in composites with fine grain alumina matrices where the fibers are protected from interface damage by various coatings show promise,[7,8] the introduction of a family of directionally solidified ceramic eutectics offer greater potential. These with well structured sub-micron scale morphology of, e.g., yttria-stabilized cubic zirconia in a topologically continuous alumina component have demonstrated great promise for both excellent creep resistance and some reasonable fracture toughness.[9] As with monolithic sapphire having a *c*-axis orientation, the key to the creep resistance of these eutectic ceramics lies with the nearly perfect *c*-axis tex-

* Corresponding author. Tel.: +1 617 253 2217; fax: +1 617 258 8742.
E-mail address: argon@mit.edu (A.S. Argon).
[1] Visiting NATO fellow. This author is on leave from the Department of Mechanical Engineering, Istanbul Technical University, Gümüssuyu 80191, Istanbul, Turkey.

0955-2219/$ – see front matter © 2005 Elsevier Ltd. All rights reserved.
doi:10.1016/j.jeurceramsoc.2005.01.022

ture of their topologically continuous alumina component,[10] which in tension again renders the best basal and prismatic slip and twinning systems unstressed. The present best evidence indicates that these eutectics creep in the 1400–1800 °C range entirely through the diffusion-controlled climb motion of both the pyramidal and prism system edge dislocations in the well textured alumina component.[11,12] Such dislocations which are surmised to have exceedingly high glide resistances should, however, experience no important restriction to climb. Here we report on the results of a new molecular dynamics (MD) study of the core structure of the $(1/3)\langle\bar{1}101\rangle$ edge dislocations on the $\{1\bar{1}02\}$ pyramidal planes to develop better insight into their diffusion controlled climb that is the central mechanism of creep in the alumina component of the Al_2O_3/c-ZrO_2 directionally solidified eutectics. In the course of the study we have also developed similar information for the $(1/3)\langle\bar{2}110\rangle$ edge dislocation on the base plane which we also present.

2. Computational details

2.1. The MOLDY computer code

The MD computations were performed with the MOLDY computer code,[13] which is in the public domain. The MOLDY code is capable of dealing with both the short range covalent interactions between ions and the long range electrostatic interactions required for Al_2O_3 The short range interactions are described by a pair potential function Φ_{ij}, between atom pairs i and j, separated by a radius vector r_{ij} of the form referred to as a Buckingham potential

$$\Phi_{ij} = -\frac{A_{ij}}{r_{ij}^6} + B_{ij}\exp(-C_{ij}r_{ij}). \quad (1)$$

The coefficients A, B and C have specific values for the O–O, Al–Al and Al–O pairwise interactions. The values of these coefficients, determined from ab initio calculations[14] are given in Table 1, together with their appropriate ionic charges. The electrostatic interactions are handled in classical Ewald sum techniques.

In the computations periodic boundary conditions were used for the simulation cells, which were in all cases chosen to be of rectangular prismatic shape. The crystallographic geometry for the simulation of dislocations on the base planes and pyramidal planes required different simulation cells, which will be introduced later. The simulations were performed in the Parinello and Rahman[15] constant stress conditions at zero external pressure. The final structures of interest were those at temperatures close to 0 K, but actual structural relaxations were usually performed at an elevated temperature (1000 K) followed by step-wise reduction of temperature to obtain stable structures at low temperatures. Equilibrated atomic structures were graphically viewed by the Atom Eye Software.[16]

Table 1
Coefficients A, B and C of the Buckingham pair potential function for α-Al_2O_3 and the appropriate electronic charges of ions used in the study[14]

Pair	A (eV Å^6)	B (eV)	C (Å^{-1})
O–O	0.49	435.63	2.7724
O–Al	0.00	3596.94	4.2283
Al–Al	675.70	9830.51	3.4638

Oxygen charge: −1.50 (e); aluminum charge: 2.25 (e).

2.2. Structure of sapphire

The standard reference for the idealized structure of α-Al_2O_3 is that of Kronberg[17] which describes the hexagonal structure as alternating layers of O ions in $\cdots$ABA$\cdots$ stacking with intervening layers of Al ions, which occupy two thirds of the interstitial sites of the O ion layers but have an $\cdots$abcabc$\cdots$ stacking. The real structure of Al_2O_3 determined first by Pauling and Hendricks[18] differs from the idealized one in an important way in which the intervening Al ions in the cation layers are alternately attracted closer to one or the other neighboring O layers where they produce small alternating local expansions of the anion interstitial sites. The one third of the vacant Al sites in the cation layers present the lowest identity translation that define the Burgers vectors of the perfect dislocations. The real ion positions have been experimentally verified by XRD by Newnham and de Haan.[19] The importance of the real ion coordinates in defining crystallographic slip and twinning processes in α-Al_2O_3 has been recently emphasized by Bilde-Sorenson et al.[20] and by Heuer et al.[21]

2.3. Choice of simulation cells

Fig. 1 shows the idealized cation sub-lattice that identifies the three principal slip systems in the Al_2O_3 structure: the basal system of $(0\,0\,0\,1)(1/3)\langle\bar{2}\bar{1}10\rangle$; the prism systems of $\{\bar{1}\bar{1}20\}(1/3)\langle\bar{1}101\rangle$ and the pyramidal system $\{1\bar{1}02\}(1/3)\langle\bar{1}101\rangle$. The lattice parameters given by Newnham and de Haan[19] were adopted for the simulations. They are: $a = 4.7589$ Å and $c = 12.991$ Å where the latter is the length of the structural unit cell,[17] as given by Fig. 1 of the cation sub-lattice. For the computational simulation there are clear advantages in choosing cells that have rectangular prismatic shapes. The two cells chosen for the simulations of the basal dislocation $(1/3)\langle\bar{2}110\rangle$ and the pyramidal dislocation $(1/3)\langle\bar{1}101\rangle$ are identified in Fig. 2 which shows a top view of the $(0\,0\,0\,1)$ base plane where the close-packed layer of O ions are identified as the large open circles. The small black circles occupying two thirds of the interstitial sites immediately above the O layer represent the Al ions while the small open circles occupying the remaining one third of the interstitial sites represent the vacant Al sites or "holes". The positioning of these cation holes prescribes the three possible Burgers vectors A_1, A_2 and A_3 of the perfect dislocations in the base plane.

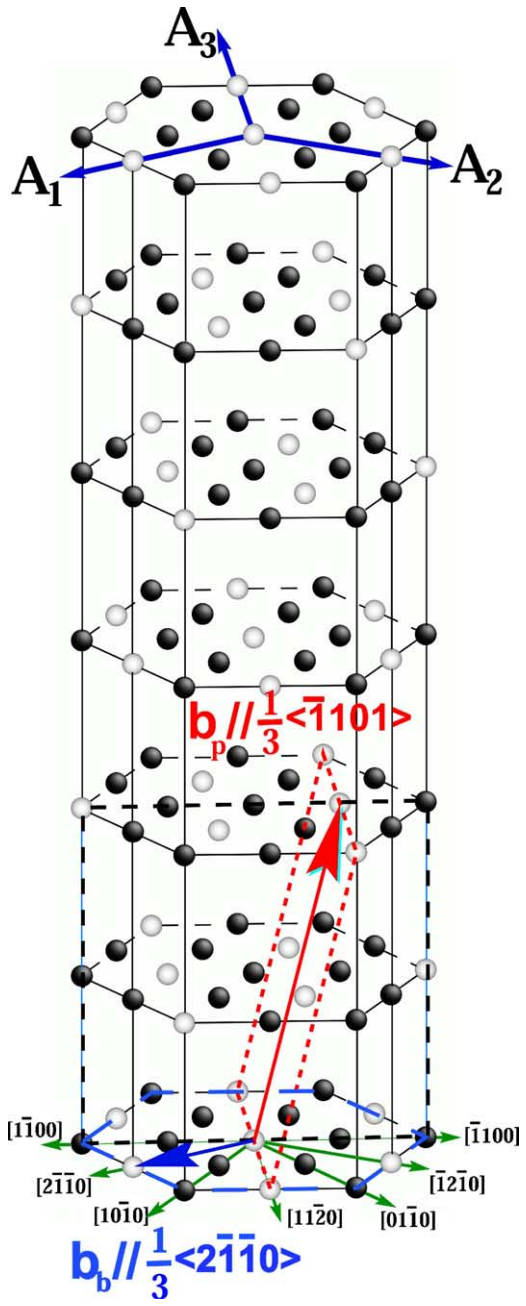

Fig. 1. The cation sub-lattice of sapphire showing the three prominent slip systems: in the basal planes (long dashed); in the prism planes (intermediate dashed); and the pyramidal planes (short dashed).

The rectangle ABCD in Fig. 2 represents the basal geometry of the simulation cell chosen for the base plane dislocation where the $[01\bar{1}0]$ direction is chosen to be parallel to the z-axis of the simulation cell of two layer thickness, The front faces of the cell consisting of the $\{01\bar{1}0\}$ planes contain the x-axis parallel to $\langle\bar{2}110\rangle$ direction and the y-axis parallel to the $[0\,0\,0\,1]$ direction. A second rectangle A′CC′ represents the geometry of the simulation cell for the pyramidal dislocation, which had its across-the-thickness z-direction parallel to the $[1\bar{2}10]$ direction of the lattice. This simulation cell was

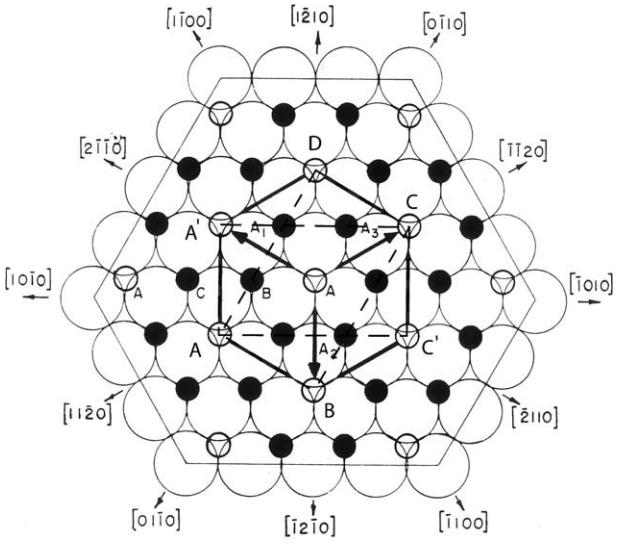

Fig. 2. The idealized arrangement of ions viewing the base plane from above $[0\,0\,0\,1]$. The large open circles represent an underlying layer of oxygen anions; the empty interstitial sites are occupied by the oxygen anion layer immediately above; the small filled circles represent aluminum cations (in the real crystal these do not lie in a single plane but are alternately associated closer to one or the other nearest oxygen layers where they produce in-plane distortions); the empty small circles represent aluminum holes which specify the scale of perfect dislocation Burgers vectors. The reference rectangle ABCD represents the base plane of the simulation cell for the base plane edge dislocation, while the rectangle AA′CC′ represents a symmetry plane in the simulation cell for the pyramidal edge dislocation (after Kronberg,[17] courtesy of Pergamon Press).

also three-layers-thick. The x and y axes of the front faces of this second simulation cell were chosen parallel to the $\langle\bar{1}101\rangle$ direction and the direction normal to the $(1\bar{1}02)$ plane, respectively, as will be clarified below when that simulation will be discussed in detail.

3. Results

3.1. Preparatory simulations

3.1.1. The perfect crystal

Prior to simulations of specific dislocation cores the MOLDY program was "tuned-in" by verifying the stability of the perfect crystal structure of sapphire. For this purpose the idealized ion coordinates given by Kronberg[17] were introduced into the perfect simulation cell for base plane dislocations and the structure was equilibrated by a MOLDY run to obtain the real ion coordinates available in the literature and the cohesive energy density of the crystal. The resulting cohesive energy at nearly 0 K was found to be $F = -96.497\,\text{eV/Al}_2\text{O}_3$ unit. The corresponding structural unit cell parameters of the perfect crystal are given in Table 2 where they are compared with some other published results. The agreement with results of other simulations and with experiments is good.

Table 2
Structural unit cell parameters of α-Al_2O_3

a (Å)	c (Å)	c/a	Source and method
4.7929	12.8333	2.678	Present study
4.7995	12.9374	2.696	Gale et al.[14] (Buckingham potential)
4.721	12.882	2.729	Marinopoulos and Elsässer,[23] (density functional method)
4.733	12.498	2.641	Marinopoulos and Elsässer,[23] (shell model)
4.7589	12.991	2.73	Newnham and de Haan,[19] (experimental)

3.1.2. Vacancy energies

In a further preparatory testing of the capabilities of the MOLDY code the anion and cation vacancies were studied. For this purpose separate studies were performed by removing an oxygen ion and an aluminum ion from the perfect crystal lattice followed by re-equilibration via a MOLDY simulation run. For both cases decreases in the volume relative to the perfect crystal were found which were $(\Delta\Omega/\Omega)_O = -2.247 \times 10^{-4}$ for the oxygen vacancy and $(\Delta\Omega/\Omega)_{Al} = -1.623 \times 10^{-3}$ for the aluminum vacancy relative to the initial perfect crystal. Clearly, these decreases in volume following the relaxations of the entire simulation cell under constant pressure indicate a collective local rearrangement of neighboring ions next to the ion that has been removed rather than the partial collapse of a spherical cavity in a continuum. The first order conventional thinking would have given an expectation of a slight volume expansion in an ionic solid where the removal of an ion with a given charge would result in a local electrostatic repulsion.[24] The fact that this was not the case indicates the dominance of local covalent interactions in Al_2O_3 over electrostatic interactions.

The corresponding vacancy formation energies were found to be $h_{fv}^{O} = 6.071\,eV$ and $h_{fv}^{Al} = 15.25\,eV$ for the oxygen and aluminum ions, respectively. These are to be contrasted with the oxygen vacancy formation energies determined by Xu et al.[25] by ab initio computations of 5.83 eV and the additive coloration experiments by Lee and Crawford[26] of 6.1 eV. No similar information was found for the Al vacancy in the literature. Based on the reasonably good agreement with other determinations for the oxygen vacancy we take our findings as acceptable even though our determination violated certain conditions of preserving charge neutrality, requiring the placement of the removed ions from the interior to a surface ledge site.[24]

3.2. Edge dislocation on the base plane

3.2.1. Core structure and line energy

While the core structure of the pyramidal edge dislocation was of primary interest in view of its role in creep of sapphire and the directionally solidified Al_2O_3/c-ZrO_2 eutectics, we have determined first the structure of the core of the basal plane edge dislocation. This structure was studied in the simulation cell with the ABCD rectangular crystallographic geometry outlined in Fig. 2, having its z-direction parallel to the [0110] direction.

To prevent formation of troubling artifacts certain conditions have to be satisfied. First, the dislocation must be introduced into the perfect lattice with correct real ionic coordinates at a symmetry plane half way between two adjacent anion layers and between the puckered cation layers associated with the anion layers around them, as has been most recently emphasized by Bilde-Sorensen et al.[20] to avoid charge imbalances. Second, dislocations must be introduced into the simulation cell as a set of dipoles with dislocation lines parallel to the short z-axis direction, [0$\bar{1}$10] of the cell to prevent formation of troublesome lattice curvatures. The procedure for this has been clarified by Cai et al.[27] where the dipole is to be placed in a configuration of an energy minimum, with the pair of dislocations roughly at 45° angles relative to their slip plane with the precise angle dependent on the conditions of the anisotropic elasticity solution for the strain fields[28] (this condition is not too critical since the capabilities in energy minimization of the MOLDY code will re-position the dislocation within the range permitted, governed by the lattice resistance). The periodic boundary conditions used in the x–y plane will generate an effective infinite dipole lattice of dislocations. Even in this case, however, the interaction energy between adjacent dipoles needs to be reduced to a minimum by choosing the aspect ratio of the simulation cell in the x–y plane correctly. The procedure for this, at least for isotropic elasticity, is well established.[29]

With the above provisos a dipole of edge dislocations was introduced into the perfect crystal cell. Fig. 3a shows the initial atom configurations around the core of the positive edge dislocation of the pair. Lines drawn through cation planes delineate the core of the introduced dislocation. Fig. 3b shows the core of this positive edge dislocation after it has been equilibrated by a MOLDY run. Examination of the lower left hand corner of the figure, considerably away from the distorted core region of the dislocation, shows some features of the real Al_2O_3 lattice ion positions. Two rows of anions and cations are visible in a somewhat overlapped position. The smaller cations that appear on top of each other are actually displaced in the z-direction and represent clearly the puckered nature of their placement in the y-direction, being alternately more closely associated with one or the other adjacent anion layers. Further examination of the placement of the two adjacent anion rows in the z-direction shows also the resulting puckered distortions in the x–z plane of the anions away from their ideal hexagonal arrangement, discussed in many structural studies.[18–21] The length of the arrow in Fig. 3a represents the length of the Burgers vector of the edge dislocation, $b = 4.7$ Å.

The line energy of the basal plane dislocation determined in the study was 10.3 eV/Å length, as half of the energy of the dipole in a characteristic simulation cell of $1.9447 \times 10^{-16}\,m^2$ area in the x–y plane and amounts to a very large dislocation density of $1.03 \times 10^{16}\,m^{-2}$. To be meaningful for a realistic case this energy needs to be scaled up to that of a more reasonable dislocation density such as $10^{12}\,m^{-2}$ that is likely to be representative of a creeping solid. This

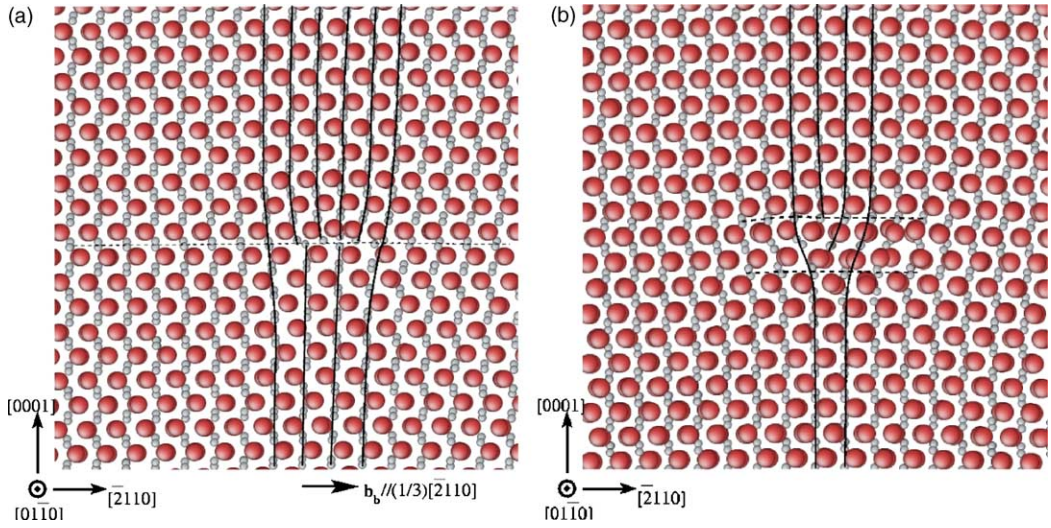

Fig. 3. (a) The initial atomic configuration of a positive edge dislocation placed on a (0 0 0 1) base plane (along the horizontal dotted line) with a Burgers vector parallel to the [$\bar{2}$110] direction into a perfect real crystal. The distorted vertical contours delineate the core region of the unrelaxed dislocation. (b) The core of the same dislocation after relaxation of the crystal with a MOLDY run, showing a central feature of the relaxation near the core where the extra half double sheet of atoms is no longer terminated on the initial base plane but is divided up into two partial edges with extra half planes terminating on two separate basal planes. Comparison of the two arrangements of the cations around the core between (a) and (b) also shows considerable tighter ionic order in the latter.

requires an increase by a factor of 2.87 to F_{DB} = 29.56 eV/Å length for the line energy, for elastic constants characteristic of those at 0 K.

3.2.2. Gamma surfaces and mobility

The mobility of a dislocation in its plane depends on the lattice resistance in that plane which opposes it. In close-packed planes where the dislocation can reduce its line energy by undergoing dissociations into partial dislocations separated by stacking faults, the lattice resistance can be substantially reduced. Such dissociations of basal dislocations in sapphire have received consideration since Kronberg.[17,20–23] While the mobility of a dissociated dislocation, particularly with the complex features of Al_2O_3 requires more detailed considerations the possibility of intermediate energy minima in building up the total Burgers displacement in a plane by partials can be gleaned from the gamma surface topography obtained by imposing rigid body translations across the plane.[30] Such a gamma surface topography for the basal plane is shown in Fig. 4. Sites A and A′ indicate interstitial sites in the oxygen sub-lattice framework of an underlying layer of oxygen ions. These interstitial sites are occupied by the oxygen ions of the layer above. The vector A–A′ corresponds to a Burgers displacement of a perfect identity translation of the upper layer of oxygen ions over the underlying one. This Burgers vector has a length of 4.75 Å. Two separate forms of dissociation into glide partials were considered by Kronberg and others.[17] The first of these is:

$$\frac{1}{3}[\bar{2}110] \rightarrow \frac{1}{3}[\bar{1}100] + \frac{1}{3}[\bar{1}010] \quad (2)$$

where the dissociation involves two Shockley type partial dislocations separated by a planar fault. This form of a two-step translation is indicated on the gamma surface of Fig. 4 as AB + BA′ with an intervening fault, which is an unsymmetrical electrostatic fault[17] of quite large energy of 0.49 eV/Å^2 (=7.84 J/m^2) suggesting that no such dissociation is likely.

Another four-fold dissociation that had also been considered is:

$$\frac{1}{3}[\bar{2}110] \rightarrow \frac{1}{9}[\bar{2}110] + \frac{1}{9}[\bar{1}2\bar{1}0] + \frac{1}{9}[\bar{2}110] + \frac{1}{9}[\bar{1}\bar{1}20] \quad (3)$$

which is indicated on the gamma surface topography of Fig. 4 as AC + CB + BD + DA′. In this dissociation a

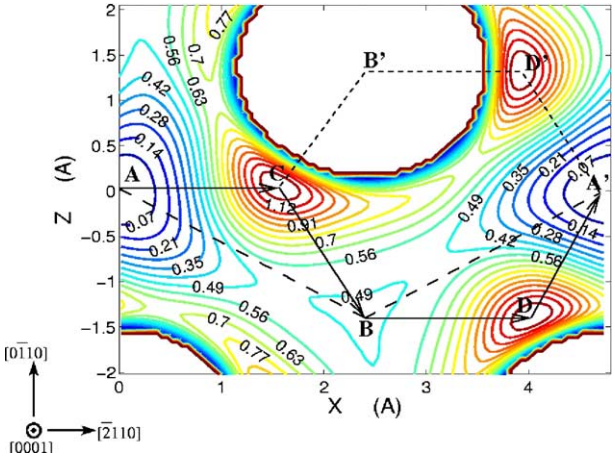

Fig. 4. The gamma surface of a representative portion of the base plane where the equi-potential contours represent potential energy levels opposing rigid body shear translation across the plane, in units of eV/Å^2. Two separate paths of possible shear from A to A′ are shown that is discussed in the text, both with rather high resistive barriers.

translation to AC produces a very high-energy stacking fault with energy 1.16 eV/Å^2 (=18.5 J/m^2) while the translation CB again positions the upper oxygen layer into an unsymmetrical electrostatic fault of energy discussed above. The further translation to BD again produces a stacking fault of the same high-energy of 1.16 eV/Å^2. Finally, the fourth translation of DA′ restores full order. Clearly, this dissociation is even more unfavorable than the first and should not occur. Parenthetically, we note that an alternative path of AC + CB′ + B′D′ + D′A′ would involve a symmetrical electrostatic fault of exceedingly high-energy that would be completely impossible.[17]

From these energetic arguments and the very narrow core shown in Fig. 3b we must conclude that no such glide dissociation can occur. Indeed there has been no experimental evidence for these dissociations. While we recognize that the levels of energy in the gamma surface plot of Fig. 4 as determined by the MOLDY computer code are likely to be quite inaccurate, these levels of energy are such that the final conclusion will remain valid.

Actually, examination of the atom positions in the relaxed core observable in Fig. 3b shows clear reconstruction of the core in a direction out of the *x*–*z* plane, above and below the base plane in the form of two partial edge dislocations with extra half planes terminating on adjacent (0 0 0 1) planes, with a clear core energy reduction. What effect this would have on the lattice resistance is unclear.

3.3. The pyramidal edge dislocation

To view the geometry of the core of the pyramidal edge dislocation simulation cells with EFGH type rectangular structural symmetry in the thickness direction $z(//[1\bar{2}10])$ were rotated around the *z*-axis to obtain a crystallographic cell with a front surface bound by the pyramidal plane $(10\bar{1}2)$ and a plane perpendicular to the $[\bar{1}011]$ direction. Fig. 5a shows a position of this cell in the perfect crystal, being viewed in the $[\bar{1}2\bar{1}0]$ direction.

The lower edge of the cell is parallel to the pyramidal $(10\bar{1}2)$ plane viewed edge-on. The slanted diagonal rows outline the nearly close-packed basal layers of oxygen ions that are divided up into packets of three, separated by the $(10\bar{1}2)$ pyramidal planes of cation holes. These potential pyramidal slip planes that contain only cation holes are designated as type "0" across which the bonding must be largely ionic. The two other potential pyramidal slip planes separating the three planes of anions in the packets are designated as type "1", across which bonding must be both of covalent and ionic nature. The character of the different bonding across these two types of planes holds the key to the expected very high glide resistance of the pyramidal system. Fig. 6a and b show that respective gamma surface of "0" and "1" type planes. The contours designate again the potential energy changes in units of eV/Å^2 experienced by the relative translation starting from the lower left hand corner in the diagram and proceeding in either the *x* $[\bar{1}011]$ direction or the *z* $[\bar{1}2\bar{1}0]$ direction or, in

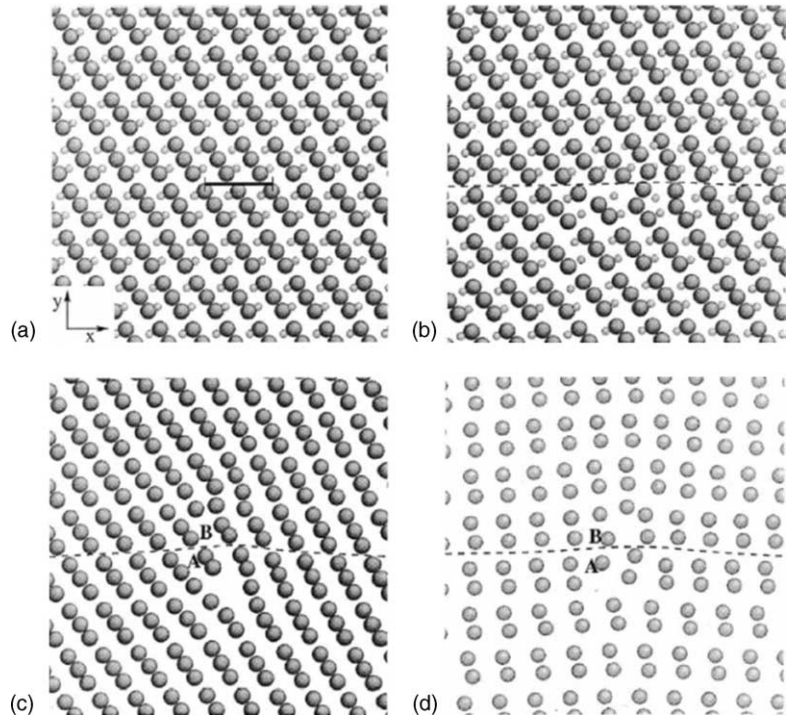

Fig. 5. The $[\bar{1}2\bar{1}0]$ view of the atomic positions in the simulation cell: (a) the positions of anions and cations in equilibrium in the perfect crystal; the bar represents the length of the pyramidal dislocation Burgers vector $b = 5.12$ Å; (b) the positions of anions and cations near a positive edge dislocation core introduced on a "0" pyramidal plane; (c) the positions of the O ions in the anion sub-lattice around the relaxed dislocation core; (d) the positions of the Al ions in the cation sub-lattice around the relaxed dislocation core.

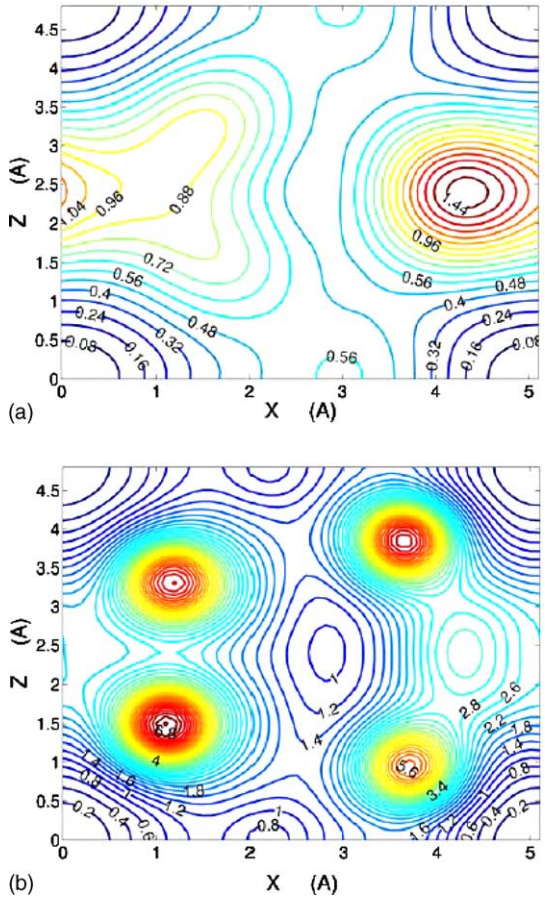

Fig. 6. The gamma surface of potential energies in units eV/Å^2, associated with rigid body shear translation across the pyramidal planes: (a) across the "0" planes of cation holes; (b) across the "1" planes having both strong covalent and ionic resistances.

any arbitrary combination. In Fig. 6a the γ-surface contours for plane "0" indicate a relatively low energy path close to the x $[\bar{1}011]$ direction parallel to the actual Burgers vector of shear translation. In comparison the gamma surface contours of Fig. 6b show no comparatively easy passage on the "1" planes in the $[\bar{1}011]$ direction.

Based on the more favorable conditions presented through the gamma surfaces a dislocation was introduced into the perfect lattice of Fig. 5a in the same procedure outlined in Section 3.2.1 for the basal dislocation. Here the procedure consisted of the introduction of an edge dislocation dipole with dislocations positioned at nearly 45° relative to the x–y system of axes of the simulation cell. The atomic surrounding of a positive edge dislocation with its $(1/3)\langle\bar{1}011\rangle$ Burgers vector lying in the "0" type plane as introduced prior to relaxation of the local environment by a MOLDY run is shown in Fig. 5b. To obtain the final core structure in the relaxed state and its energy, a special procedure consisting of equilibration at 1000 °C followed by "slow annealing" was adopted. The final core structures, which are best viewed in the separate anion and cation sub-lattices are presented in Fig. 5c and d, respectively. The final line energy of the relaxed pyramidal edge dislocation was found to be $F_D^r = 5.4633\,\mathrm{eV}/\mathring{A}$ length.

Again this energy in the dipole lattice corresponds to a very high dislocation density of $\rho = 5.35 \times 10^{16}$. To relate it to a more representative steady state dislocation density of 1.1×10^{12} encountered in creep experiments[5] at a stress of 135 MPa, the energy must be scaled up by a factor of about 3.10 or to $F_D = 17.0$ eV/Å. We note that this energy is only 0.53 of the line energy of the $(1/3)\langle\bar{2}110\rangle$ basal dislocation in spite of the fact that the pyramidal edge dislocation has a Burgers vector that is 1.078 times longer than the base plane Burgers vector of 4.75 Å. This requires that to first order considerations the shear modulus across the pyramidal plane in the Burgers vector direction would be correspondingly lower than that of the base plane. A standard coordinate axis transformation gave indeed that the ratio μ_p/μ_b of the shear moduli of the pyramidal plane to the base plane was 0.7 giving $(\mu b^2)_p/(\mu b^2)_b$, and considerably closer to unity, with the remaining difference, no doubt being attributable to the more complex dependence of the line energies on other anisotropic components of the elastic compliance tensor. Fig. 5c and d show that in the relaxed equilibrium form the core of the pyramidal dislocation had undergone an important alteration. Instead of the termination of the pair of extra half planes remaining on the type "0" pyramidal plane of cation holes the dislocation core had undergone a dissociation into two partial edge dislocations of half strength which have been displaced vertically into two adjacent type "1" pyramidal planes. However, according to the gamma surface topography of Fig. 6b the type "1" planes should be quite unfavorable to any glide mobility of these dislocations due to the strong combined covalent and ionic bonding across them, unlike the "0" plane which should have only weak bonding across it. Since the two extra half planes are composed of both anions and cations the dissociation and rearrangements in the core are complex. They are viewed best in the individual anion and cation lattices of Fig. 5c and d. In the anion lattice of Fig. 5c, the pair of O ions designated as "A" have descended from the site indicated as "B". This has relieved both the high compressive stresses at the immediate termination of the pair of extra half planes of the unrelaxed configuration and has also reduced the high tensile stresses on the opposite side. Correspondingly, a different but energetically similar rearrangement has occurred in the cation sub-lattice shown in Fig. 5d, where Al ions "A" and "B" that must have had positions "A–B" (from left to right) at the terminus of the pair of extra half planes have undergone a counter clockwise shuffle, placing ion "A" below the "0" plane and thereby permitting ion "B" to move toward the left. In both cases the new positions of ions "A" and "B" have accomplished the same function of relieving the large tensile and compressive stresses of the termination of the two extra half layers by effectively "feathering-in" the blunt wedge into a sharper, better fitting one. Thus, while the configuration of the initial unrelaxed state of Fig. 5b is artificial and its energy is not effectively determinable by MD, the energy of the final relaxed configuration of Fig. 5c and d must represent a substantial improvement in the core energy. We note an interesting parallel with the case of the Ll_2

type ordered alloys such as Ni_3Al, where the super dislocations on the principal $\{1\,1\,1\}$ glide planes can undergo a thermally activated cross slip into $\{0\,1\,0\}$ cube planes where the energy of the dislocations is substantially reduced due to reductions in the antiphase boundary energy on those planes. This, however, drastically reduces the mobility of the dislocation in the $\{0\,1\,0\}$ plane.[31] As noted above, in the relaxed configuration of the dislocation core with its vertical dissociation and placement of the two partial dislocations in type "1" pyramidal planes, it is clear that these dislocations will be essentially immobile for glide. However, the structural alterations in the cores of the pyramidal dislocations should have little influence on their climb motion.

4. Discussion

Of the core structures of the base plane dislocation and the pyramidal dislocation the latter is of primary interest from the point of view of creep in the Al_2O_3 component of the directionally solidified Al_2O_3–ZrO_2 eutectics where this component has a remarkably tight [0 0 0 1] growth texture that renders all but the pyramidal slip system unstressed. Moreover, the findings of Section 3.3 indicate that the pyramidal dislocation should be incapable to glide by virtue of its core restructuring. In connection with the sessile core configuration of Fig. 5c and d a reverse thermally activated process might be considered in which glide on the "0" planes becomes possible if thermal fluctuations can momentarily reverse the dissociation of the core and place both partial dislocations back together into the type "0" plane where short steps of advancement might become possible before the dislocation core again relaxes to its trapped from of lower core energy at a neighboring site. Models of this type where a dislocation line, locked in a potential trough, is liberated under stress have been considered in detail for a number of similar applications.[32,33] For our case the required activation free energy ΔG^* of thermally assisted release under a resolved shear stress σ, of a dislocation line bound into a potential trough of depth ΔF per unit length and half width δ, is readily obtainable as[33]

$$\Delta G^* = \frac{4}{3}(F_D\delta)\left(\frac{3+\beta}{\beta}\right)\sqrt{2\alpha(1-\beta)} \tag{4}$$

where $F_D \cong F_D^r$ is the line energy per unit length of the free dislocation on the "0" plane, $\beta = \sigma/\hat{\tau}$, $\alpha = \Delta F/F_D$ and $\hat{\tau} = \Delta F/b\delta$ is the athermal resolved shear stress to tear the dislocation out of the potential trough. For the high stress limit to which we expect to be near

$$\Delta G^* \cong \frac{16}{3}\sqrt{2\alpha}(F_D\delta)\left(1-\frac{\sigma}{\hat{\tau}}\right)^{1/2} \tag{5}$$

for a guessed $\alpha = 0.1$, $\delta \approx b = 5.12$ Å and $F_D \approx 17.0$ eV/Å as determined above and for a maximum possible level of thermal fluctuation of 10 eV at, say, 1800 K we find that σ cannot differ from $\hat{\tau}$ by more than 0.2% or would have to be near 10 GPa—an impossible condition to satisfy. Thus, the pyramidal edge dislocation must indeed be tightly bound to the lattice and cannot glide.

We must conclude, then that creep in the eutectics will have to be entirely by the climb of the pyramidal and possibly also the prism plane edge dislocations. Theoretical models for such creep can readily be developed by a variant of a model presented by Firestone and Heuer.[5] Such a creep model together with associated creep experiments on the eutectic of Al_2O_3/c-ZrO_2 is presented in a companion communication.[12] The only remaining question is the source of and the structure of jogs on the pyramidal dislocations where the actual climb steps take place. Energetic arguments similar to the one given above for the thermally activated glide indicate that jogs that are expected to be complex cannot be generated by thermal fluctuations at any meaningful rate, but must be produced from nodes in the climbing network of dislocations.[12]

Acknowledgments

This research was supported by the AFOSR under grant F69620-99-1-0276, and by a NATO Science Fellowship (to C.T.B.) from the Science and Technical Research Council of Turkey (TUBITAK). We acknowledge useful discussions with Professors B. Wuensch of M.I.T. and A.H. Heuer of Case Western Reserve University on the relaxed real coordinates of ions in sapphire. For the computations we used the resources of Professor S. Yip of M.I.T.

References

1. Fleischer, R. L., High-strength, high-temperature intermetallic compounds. *J. Mater. Sci.*, 1987, **22**, 2281–2288.
2. Rice, J. R., Beltz, G. E. and Sun, Y., Peierls framework for dislocation nucleation from a crack tip. In *Topics in Fracture and Fatigue*, ed. A. S. Argon. Springer-Verlag, New York, 1992, pp. 1–58.
3. Lawn, B., *Fracture of Brittle Solids* (*2nd ed.*). Cambridge University Press, Cambridge, EUK, 1995.
4. Burton, B., Diffusional creep of polycrystalline materials. *Diffusion and Defect Monograph Series-5*. Trans Tech Publishers, Bay Village, OH, 1977.
5. Firestone, R. F. and Heuer, A. H., Creep deformation of 0 degree sapphire. *J. Am. Ceram. Soc.*, 1976, **59**, 24–29.
6. Farmer, S. C. and Sayir, A., Tensile strength and microstructure of Al_2O_3/c-ZrO_2 hypo-eutectic fibers. *Eng. Fract. Mech.*, 2002, **69**, 1015–1024.
7. Morgan, P.-E.-D. and Marshall, D. B., Ceramic composites of monazite and alumina. *J. Am. Ceram. Soc.*, 1995, **78**, 1553–1563.
8. Lev, L. C. and Argon, A. S., Oxide-fiber/oxide-matrix composites. *Mater. Sci. Eng. A*, 1995, **195**, 251–261.
9. Pastor, J. Y. *et al.*, Mechanical properties of directionally solidified Al_2O_3/c-ZrO_2(Y_2O_3) eutectics. *Mater. Sci. Eng. A*, 2001, **308**, 241–249.
10. Frazer, C. S., Dickey, E. C. and Sayir, A., Crystallographic texture and orientation variants in Al_2O_3/$Y_3Al_5O_{12}$ directionally solidified eutectic crystals. *J. Crystal Growth*, 2001, **233**, 187–195.
11. Argon, A. S., Yi, J. and Sayir, A., Creep resistance of directionally solidified ceramic eutectics of Al_2O_3/c-ZrO_2 with sub-micron

columnar morphologies. *Mater. Sci. Eng. A*, 2001, **319–321**, 838–842.
12. Argon, A. S., Yi, J. and Sayir, A., Creep resistance of the directionally solidified ceramic eutectic of Al_2O_3/c-ZrO_2(Y_2O_3): experiments and models. *J. Eur. Ceram. Soc.*, 2005, **25**, 1201–1214.
13. Refson, K., MOLDY: a portable molecular dynamics simulation program for serial and parallel computers. *Comput. Phys. Commun.*, 2000, **126**, 310–329.
14. Gale, J. D., Catlow, C. R. A. and Mackrodt, W. C., Periodic ab initio determination of interatomic potentials for alumina. *Model. Simul. Mater. Sci. Eng.*, 1992, **1**, 73–81.
15. Parinello, M. and Rahman, A., Polymorphic transitions in single-crystals—a new molecular-dynamics method. *J. Appl. Phys.*, 1981, **52**, 7182–7190.
16. Li, J., Atom Eye: an efficient atomistic configuration viewer. *Model. Simul. Mater. Sci. Eng.*, 2003, **11**, 173–177.
17. Kronberg, M. L., Plastic deformation of single crystals of sapphire, basal slip and twinning. *Acta Metall.*, 1957, **5**, 507–524.
18. Pauling, L. and Hendricks, S. B., The crystal structures of hematite and corundum. *J. Am. Chem. Soc.*, 1925, **47**, 781–790.
19. Newnham, R. E. and de Haan, Y. M., Refinement of the αAl_2O_3, Ti_2O_3, V_2O_3 and Cr_2O_3 structures. *Z. Kristallogr.*, 1962, **117**, 235–237.
20. Bilde-Sorenson, J. B. *et al.*, On basal slip and basal twinning in sapphire (α-Al_2O_3)—I. Basal slip revisited. *Acta Mater.*, 1996, **44**, 2145–2152.
21. Heuer, A. H., Lagerlöf, K. P. D. and Castaing, J., Slip and twinning dislocations in sapphire (αAl_2O_3). *Phil. Mag.*, 1998, **78**, 747–763.
22. Marinopoulos, A. G., Nufer, S. and Elsässer, C., Interfacial structures and energetics of basal twins in α-Al_2O_3: first-principles density-functional and empirical calculations. *Phys. Rev. B*, 2001, **63**, 165112–165119.
23. Marinopoulos, A. G. and Elässer, C., Density-functional and shell-model calculations of the energetics of basal-plane stacking faults in sapphire. *Phil. Mag. Lett.*, 2001, **81**, 329–338.
24. Friedel, J., *Dislocations*. Pergamon Press, Oxford, England, 1964.
25. Xu, Y.-N., Gu, Z.-Q., Zhong, X.-F. and Ching, W. Y., Ab initio calculations for the neutral and charged O vacancy in sapphire. *Phys. Rev. B.*, 1997, **56**, 7277–7284.
26. Lee, K. H. and Crawford Jr., J. H., Additive coloration of sapphire. *Appl. Phys. Lett.*, 1978, **33**, 273–275.
27. Cai, W., Bulatov, V. V., Chang, J., Li, J. and Yip, S., Periodic image effects in dislocation modeling. *Phil. Mag.*, 2003, **A83**, 539–567.
28. Hirth, J. P. and Lothe, J., *Theory of Dislocations* (*2nd ed.*). McGraw-Hill, New York, NY, 1982.
29. Chang, J., *Atomistics of Defect Nucleation and Mobility; Dislocations and Twinning*. Ph.D. thesis, Massachusetts Institute of Technology, Cambridge, MA, 2003.
30. Vitek, V., Intrinsic stacking faults in body-centered cubic crystals. *Phil. Mag.*, 1968, **18**, 773–786.
31. Paidar, V., Pope, D. P. and Vitek, V., A theory of the anomalous yield behavior in Ll_2 ordered alloys. *Acta Metall.*, 1984, **32**, 435–448.
32. Fisher, J. C., Application of Cottrell's theory of yielding to delayed yield in steel. *Trans. ASM*, 1955, **47**, 451–462.
33. Kocks, U. F., Argon, A. S. and Ashby, M. F., Thermodynamics and kinetics of slip. In *Prog. Mater. Sci., vol. 19*, ed. B. Chalmers, J. W. Christian and T. B. Massalski. Pergamon Press, Oxford, 1975, pp. 1–281.